

Article

Estimation Procedure for the Degradation of a Lithium-Ion Battery Pack

Natascia Andrenacci ^{1,*}, Manlio Pasquali ¹, Francesco Vellucci ¹ and Alberto Venanzoni ²

¹ Sustainable Mobility and Transport Laboratory, Casaccia Research Center, ENEA, via Anguillarese, 00193 Rome, Italy; manlio.pasquali@enea.it (M.P.); francesco.vellucci@enea.it (F.V.)

² Enel X, Viale di Tor di Quinto 45/47, 00191 Rome, Italy; alberto.venanzoni@enel.com

* Correspondence: natascia.andrenacci@enea.it

Abstract: This paper proposes a test procedure for evaluating the degradation of cells in a battery pack. The test can be performed using only the charger's converters and the battery management system (BMS) without requiring sophisticated instrumentation. The method circumvents the difficulties related to the evaluation of derivative quantities for estimating the state of health (SOH) using integral quantities in the evaluation. The method introduces a ‘degradation function’ that is calculated with respect to the reference performance of pristine cells. The procedure was applied to the JuiceRoll Race Edition system, an innovative electric vehicle (EV) DC charger with internal storage, made in ENEL X and used during the MotoE championship races. Using this procedure, the degradation of performance in individual groups of cells composing the battery pack was quantified in comparison to the reference group. The procedure helps identify modules that have aged too early or show reliability issues. The method is mature for field operational applications.

Keywords: battery module; state of health; battery diagnostic



Citation: Andrenacci, N.; Pasquali, M.; Vellucci, F.; Venanzoni, A. Estimation Procedure for the Degradation of a Lithium-Ion Battery Pack. *Batteries* **2024**, *10*, 234. <https://doi.org/10.3390/batteries10070234>

Academic Editors: Chris Mi and Wei Gao

Received: 24 May 2024

Revised: 21 June 2024

Accepted: 24 June 2024

Published: 28 June 2024



Copyright: © 2024 by the authors. Licensee MDPI, Basel, Switzerland. This article is an open access article distributed under the terms and conditions of the Creative Commons Attribution (CC BY) license (<https://creativecommons.org/licenses/by/4.0/>).

1. Introduction

Batteries are a crucial component of electrical systems and electronic devices. As such, they have a significant role in addressing the challenges associated with increasing global energy consumption and climate change. Among various types of batteries, lithium batteries are highly valued for their long-life, high-energy, and high-power characteristics [1]. These batteries are an essential part of systems like electric cars or microgrids. Therefore, it is imperative to manage batteries efficiently to extend their lifespan, enhance reliability, and reduce costs. To achieve this, it is essential to have accurate knowledge and prediction of the battery’s state of health (SOH) [1,2]. A short-term health prognosis for estimating capacity is the focus of the SOH [3]. Monitoring the SOH of a battery is extremely important for the battery management system (BMS). The BMS is responsible for optimally managing the energy storage system’s performance while protecting it from damage resulting from operations outside of its limits. A timely evaluation of the SOH of the battery cells allows the prompt optimization of the system and extension of the life of the entire battery pack [4]. The SOH of a battery is usually described as the battery performance at present compared with the performance at ideal conditions or the beginning of the battery life. As such, there is no unique operational definition of SOH, but it usually depends on the battery applications. The estimation of a battery’s SOH can take into consideration both the capacity fade and the impedance increase. The extraction and selection of quantities to evaluate battery health is crucial for accurate predictions of SOH and remaining useful life (RUL) [5]. Several other variables can be considered for the SOH evaluation [6]. Most refer to derivative variables that require precise estimates, which are particularly prone to measurement and propagation errors in calculations.

Various methods can be used to estimate the state of charge (SOC) and SOH, each with its advantages and limitations. They can be classified as data-driven, model-driven, and

hybrid approaches [7]. The model-driven approach includes empirical models, equivalent circuit models (ECMs), and electrochemical models (EMs). The first approach relies on an empirical relationship between the SOH and the influencing factors obtained through experiments. The ECM uses representative electrical elements to describe battery behavior, while the EM employs first principles to represent the internal physicochemical reactions via differential equations. The complexity and accuracy of these models are inversely proportional. Indeed, EM approaches proved to be useful in the detection of differences between nominal and faulty status, but they are usually computationally demanding, although a reduction in the dimensionality can be useful if integrated with degradation modes [8,9]. Equivalent circuit models are simpler models that have been used to evaluate the SOH [10], state of power [11], and SOC [12]. A data-driven, machine learning-based approach is model-free and attempts to map the non-linear relationship between selected inputs and the SOH. However, one of the main disadvantages of machine learning-based methods is the lack of a physical explanation. Machine learning, unsupervised, and deep learning techniques have been used to predict RUL and SOH based on different parameter measurements [13–16]. These approaches can provide very accurate results even with noisy measurements [17]. A multi-model integration of physical models and a data-driven approach were successfully used for the SOC and SOH estimation [18,19]. Even though data-driven approaches demonstrate accuracy, they require a large amount of data for training, and they are unreliable in extrapolating results outside the training range.

Faults in batteries can be diagnosed by monitoring the voltage [20], especially investigating the features of the incremental capacity (IC) and differential voltage (DV) curves [21,22]. A combination of these approaches is also reported in the literature [23–25]. Additionally, the maximum available energy has been proposed as an indicator for battery SOH [26]. The correlation between battery open-circuit voltage (OCV) and SOC changes as the battery degrades and it is, therefore, a possible indicator of battery SOH [27]. Statistical approaches are also used to evaluate the battery ageing process through SOC-OCV evolution [28].

Since the actual operating environments of batteries can be relatively extended, some SOH evaluation approaches are based on actual operating parameters, rather than laboratory measurements. Vichard et al. [29] propose a method based on an experimental database from a three-year monitoring period of a fleet of ten experimental fuel cell hydrogen electric vehicles equipped with Li-ion batteries to model batteries against operating conditions. They focus on the evaluation of the capacity using the Kalman filters approach. In [30], they propose an online method for estimating the SOH based on the charging data of electric vehicles in normal working conditions. The main goal of the model is the estimation of complete charging parameters starting from partial charges and using historical data on complete and partial charges. Hong et al. [31] propose a deep learning-based method based on the correlation between battery degeneration factors and various vehicle operating parameters, obtaining an approximate battery degeneration model oriented towards real application scenarios. These methods rely on data-driven approaches or require the evaluation of parameters from instantaneous quantities. In [4], the instantaneous discharge voltage and its derivatives with respect to time, V' , are used as variables to determine the SOC and SOH. The SOH was found to be linear with $1/V'$ by a modification factor that is a function of the SOC. An adaptive run-time circuital model is used in [32] for real-time performance evaluation of an energy storage system in a highly dynamic application.

The work presented in this paper also aims to utilize data from battery storage operations to evaluate performance degradation. Unlike previous studies, the proposed approach examines the performance of the individual modules within the battery pack, instead of focusing on the overall battery pack. This method does not rely on data from previous measurements, but only on the definition of nominal and end-of-life values for the relevant battery's variables.

Another difference from previous similar studies is that the degradation evaluation procedure proposed in the present work shifts the problem from quantifying the parameters

of a circuit to measuring their effects on a duty cycle. As such, the comparison is made between different cells or modules of the battery under investigation, without referring to pre-existing measurements or underlying degradation models. Moreover, it is designed to be performed using the charger's converters and the BMS, without requiring sophisticated instrumentation, and can be performed during normal battery operations.

In particular, the proposed procedure applies to battery packs built of modules in series, each one composed of a parallel set of *a priori* identical cells. In this context, the proposed procedure characterizes each module with a numerical value from an index that describes its state of health/degradation compared to a 'nominal' health/degradation reference and the maximum acceptable degradation: for index values higher than the maximum admissible value, the module must be replaced.

The main characteristic of the approach is that it is based on procedures that satisfy the following criteria:

- They are designed to be simple and easy to perform, requiring only basic tools and equipment.
- They are non-destructive and do not require any disassembly of the battery pack.
- They can be used to identify a variety of battery health issues, including capacity fade, impedance increase, and cell imbalance.
- They can be used to track the health of the battery pack over time and identify any groups that may need to be replaced.

The main benefits of the approach include the following:

- It helps to ensure the safe and reliable operation of the battery pack.
- It helps to extend the life of the battery pack.
- It helps to reduce the cost of battery pack maintenance.

In the following sections, we introduce the variables and define the test procedures to evaluate the proposed performance index. We then illustrate an application to a real-world case study, using an ad hoc test to monitor battery storage integrated into the system called the JuiceRoll Race Edition. Finally, we discuss the outcomes of the work.

2. Materials and Methods

Below, we present some test procedures for measuring the health status of a battery pack that can be carried out directly using only the charger's converter and the BMS, without, therefore, requiring sophisticated instrumentation. First, we give a general definition of the battery packs that can be monitored with the proposed approach. Then, we introduce the equivalent circuit model (ECM) and the test procedure for the determination of the ECM parameters, along with the main variables that characterize the definition of SOH.

2.1. Battery Pack

We consider a generic battery pack composed of a group of ideally identical cells connected in parallel and then connected in series with other identical groups, as shown in Figure 1.

During assembly, the cells differ, at most, in manufacturing tolerances. As they age, their characteristics decay, potentially unevenly. Furthermore, the package may have manufacturing defects or be damaged during transportation, assembly, or use: these conditions could result in performance degradation or safety problems, such as short circuits.

The performance and safety of a battery pack are influenced by the characteristics of the most degraded cell or by the defects mentioned above: for this reason, it is important to identify the degradation both in diagnostics and in the prediction of performance loss.

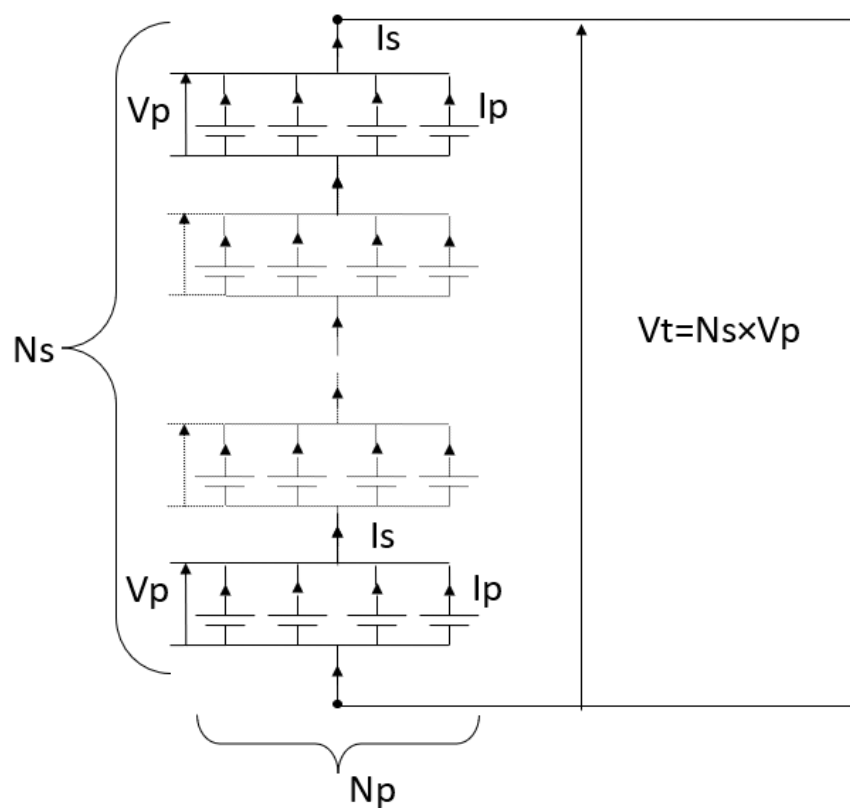


Figure 1. Battery pack assemblage.

2.2. Equivalent Circuit Model

It is possible to create an equivalent circuit model (ECM) that is equivalent to the entire pack, with each group of cells connected in parallel (module), or a single cell. For our purposes, we decided to model a module as a single element.

A widely used circuit model for representing a battery is the one shown in Figure 2.

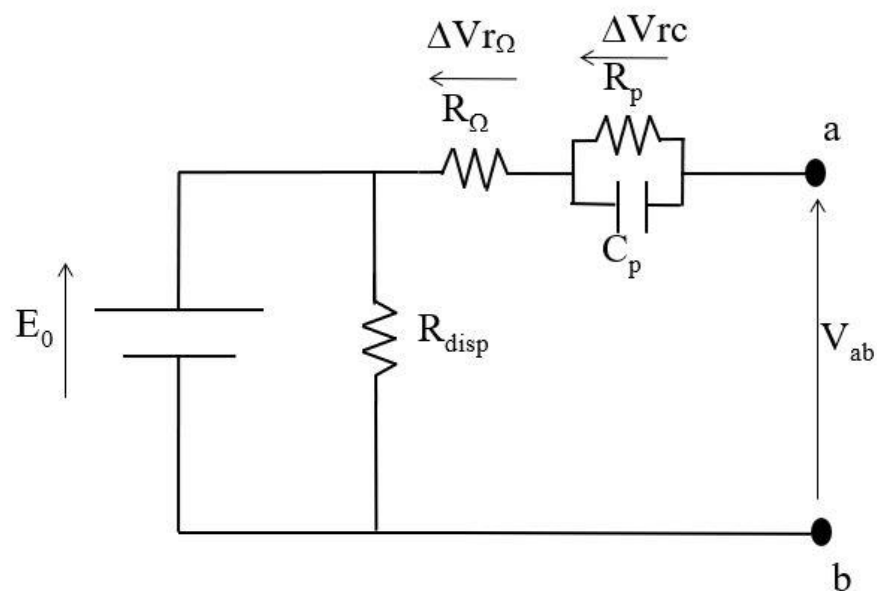


Figure 2. Generic equivalent model of a battery.

R_{disp} represents the self-discharge contribution, R_Ω is the ohmic contribution, and the single parallel $R_p C_p$ branch represents the dynamic response of the battery. E_0 represents

the open-circuit electromotive force in stationary conditions: the battery voltage, V_{ab} , coincides with E_0 when the current flowing in the circuit is zero. All parameters are a function of the battery state of charge (SOC).

The SOC is defined as a function of the nominal capacity C_{nom} of the battery, provided by the manufacturer:

$$SOC = 1 - \frac{Q_e}{C_{nom}} = 1 - \frac{1}{3600} \frac{\int_0^t i(t) dt}{C_{nom}} \quad (1)$$

where $Q_e = \frac{1}{3600} \int_0^t i(t) dt$ is the amount of charge stored in the battery at time t , expressed in ampere-hours (Ah), and $i(t)$ is the charging current. The circuit model in Figure 2 allows identification of the no-load voltage, the energy and power that can be absorbed/delivered by the battery, the maximum short-circuit current, and the temporal response to a load request. The state of health or degradation of a cell depends on the variation in the numerical values of the model parameters compared to the nominal ones. The state of health or degradation is, therefore, related to the characteristics of a battery in nominal conditions, i.e., $SOH = 1$, when the characteristics of the battery under examination are identical to the reference one.

Table 1 reports the impact on performances of the ageing of the ECM components.

Table 1. Degradation mechanisms and impacts on performance.

| Ageing Effects | Impacts on Performance |
|-----------------------------------|--|
| Capacity reduction | Reduction in the storable energy |
| Increasing of internal resistance | Increased energy dissipation, decreased efficiency |
| Increasing of internal impedance | Increased transient time |
| Open voltage reduction | Reduction in the storable energy |

2.3. Standard Charge–Discharge

Figure 3 shows the standard discharge–charge cycle for an elementary cell, used to measure its effective capacity.

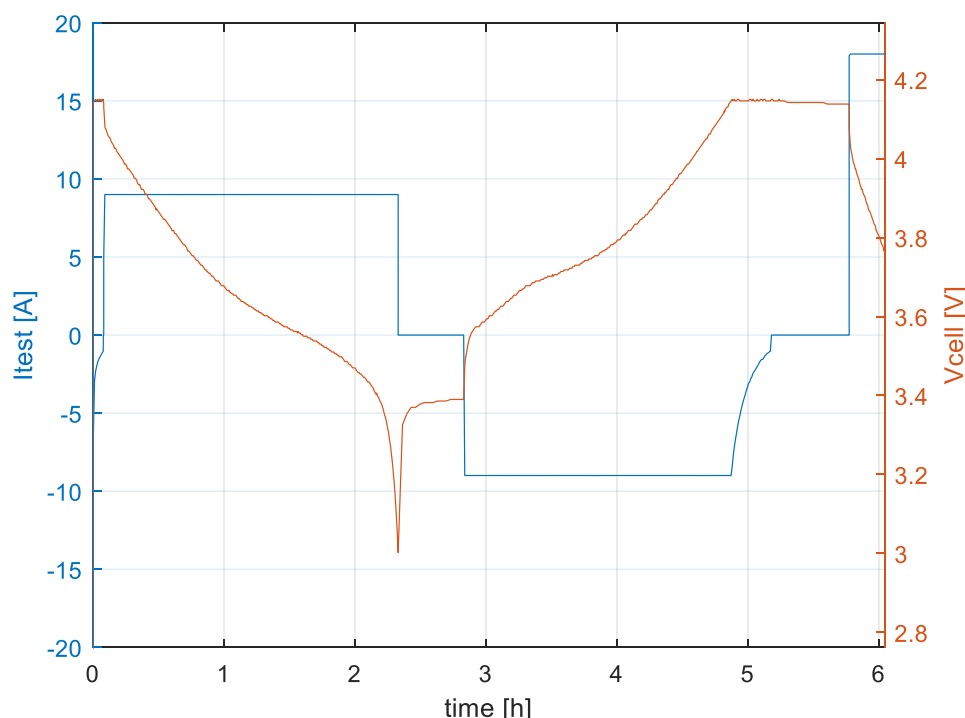


Figure 3. Standard discharge–charge profile.

At the beginning of the test, the cell is at rest, and its voltage is equal to the electromotive force E_0 , which is equivalent to V_{cmax} and corresponds to SOC = 1. Then, the cell is discharged with a constant current equal to a 0.5 C rate (1 C rate corresponds to the current needed to discharge completely (from SOC = 1 to SOC = 0) a battery in 1 h), until its voltage reaches V_{cmin} , which is the minimum working voltage as provided by the manufacturer. After that, the current is set to zero, and the cell is left to rest until the no-load voltage matches E_0 . Next, the cell is charged at a 0.5 C rate until the voltage reaches V_{cmax} again. Then, the charging process continues at a constant cell voltage, with the current being gradually decreased (constant-voltage charging, CV). The test finishes when the current drops below a pre-established minimum value, indicated by the manufacturer or the relevant standards, and the cell is considered fully charged.

The capacity is then determined by the integral of the current over the discharge time interval (Equation (2)).

$$C_{eff} = \frac{1}{3600} \int_{t_0}^{t_{dsc}} i \, dt \quad (2)$$

Other quantities that can be introduced are the amperometric efficiency (Equation (3)) and the energetic efficiency (Equation (4)):

$$\eta_A = \frac{\int_0^{T_{scar}} i_{scar} dt}{\int_0^{T_{car}} i_{car} dt} \quad (3)$$

$$\eta_E = \frac{\int_0^{T_{scar}} V_c i_{scar} dt}{\int_0^{T_{car}} V_c i_{car} dt} \quad (4)$$

During the standard charge and discharge test, the quasi-stationary conditions make it possible to ignore the impact of the circuit's capacity, except for the pause phase that follows the discharge. During this time, the voltage rise is influenced by the impedance of the RC branch. However, this phenomenon has no bearing on the effective capacity calculation. The limited pause time of a few hours allows the disregarding of the cell self-discharge. As a result, the ECM depicted in Figure 2 reduces to that of Figure 4.

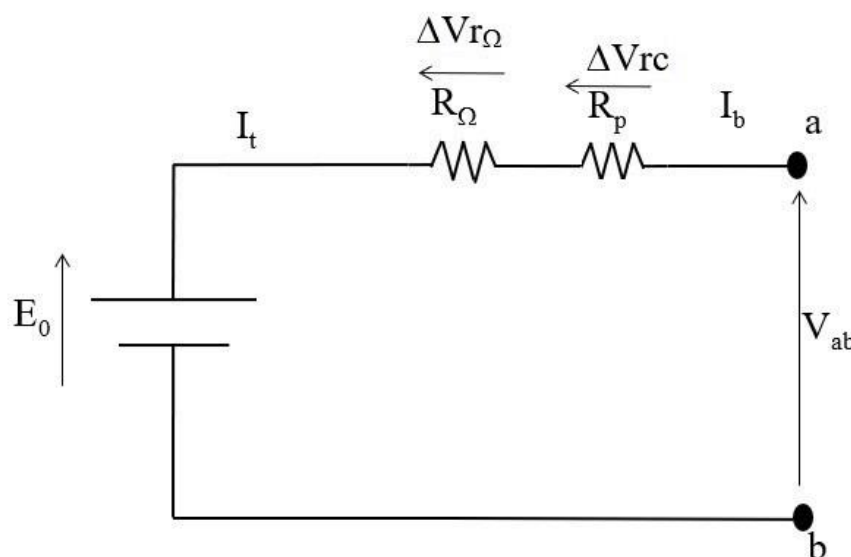


Figure 4. Simplified equivalent circuit model.

For the purposes of this study, an alternative formulation of the SOC will be used, where the nominal capacity in Equation (1) is replaced with the effective capacity, as defined by Equation (2):

$$SOC = 1 - \frac{Q_e}{C_{eff}} \quad (5)$$

The corresponding depth of discharge (*DOD*) is defined as

$$DOD = 1 - SOC = \frac{1}{3600 C_{eff}} \int_{t_i}^t i(t) dt \quad (6)$$

We introduce the area A_c included in the closed curve *DOD* vs V_{ab} , shown in Figure 5, defined as

$$A_c = \int_{DOD_i}^{DOD_f} V_{ab}(t) d(DOD(t)) dt \quad (7)$$

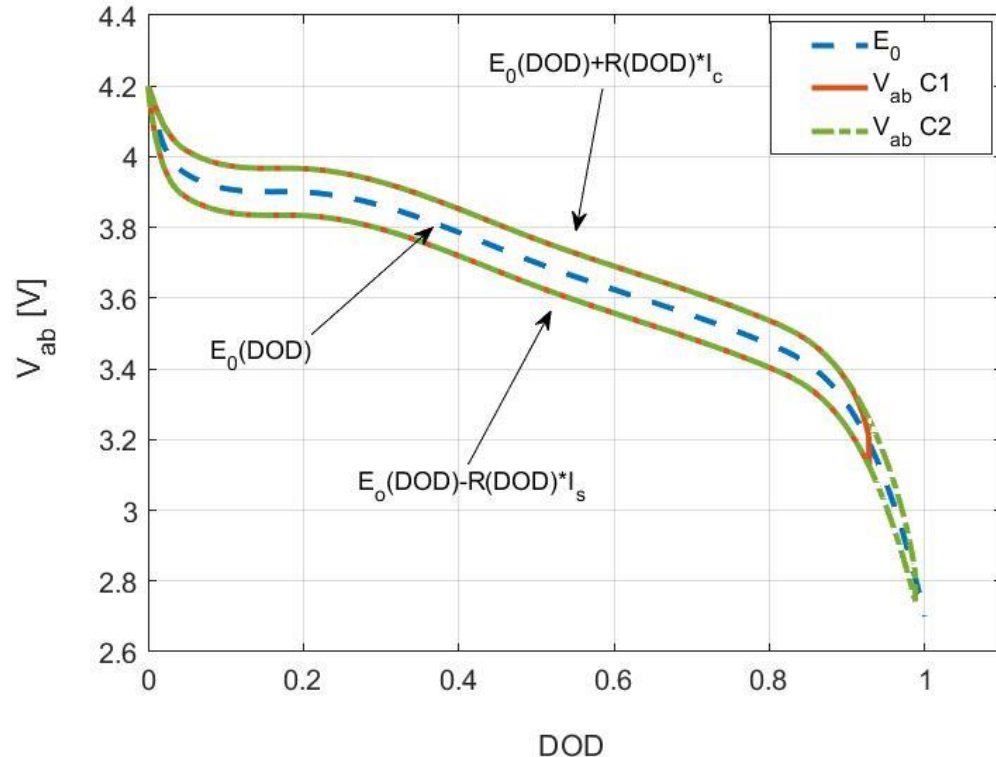


Figure 5. Comparison among areas for differently aged cells. The cell 1 capacity is bigger than the cell 2 one: $C_1 > C_2$. (* stands for multiplication sign).

Using the simplified ECM, it is immediately possible to interpret the meaning of the A_c area obtained from the standard test: the upper curve, corresponding to the charge, is given by

$$V_c(DOD) = E_0(DOD) + R_c(DOD)I_c \quad (8)$$

where $R_c(DOD) = R_{\Omega,c}(DOD) + R_{p,c}(DOD)$ is the total internal resistance, and I_c is the charge current.

The lower curve corresponds to

$$V_d(DOD) = E_0(DOD) - R_d(DOD)I_d \quad (9)$$

where I_d is the discharge current, and $R_d(DOD)$ is the internal resistance. In general, $R_d(DOD) \neq R_c(DOD)$.

Consider a set of serially connected modules composed of cells connected in parallel. These modules undergo a standard discharge and recharge, starting from the same initial conditions between the cells. If the cells have different capacities and internal resistances, the discharge will be interrupted by the cell with the lower capacity or the higher internal resistance. As a result, the DOD values for each module will be inversely proportional to their effective capacities. Consequently, the A_c area value is inversely proportional to the effective capacity of the module and proportional to its series resistance, as shown in

Figure 5. Therefore, the A_c area associated with a cell or module in given conditions is lower than that of a more degraded cell or module.

The proposed procedure replaces the point estimation of the cell resistance with the measurement of its effects on the system performance. However, it is necessary to have an initial estimate of the cell's open-circuit voltage and its series resistance. It is possible to evaluate these quantities in an approximate way from the information provided by the manufacturer, which directly provides the trend of E_0 at no load as a function of the SOC, or that relating to the V_{ab} for different discharge rates of the cell.

2.4. Description of the Procedure

The battery pack is assembled according to the requirements of the application and the technical characteristics of the cells, provided by the manufacturer's Data Sheet. The battery pack considered in this work consists of a set of identical modules, each made up of a certain number of cells in parallel, connected in series to each other. Depending on the application, the maximum acceptable value of degradation of the pack's performance is defined in terms of a reduction in effective capacity and an increase in the series resistance of a single cell or module. In the absence of a design choice, the following choice is conventional for the automotive sector:

$$C_{eol} = 0.8C_{nom}, \quad (10a)$$

$$R_{s,eol} = 2 R_{s,nom}. \quad (10b)$$

where C_{eol} , $R_{s,eol}$ are the numerical values of the capacity and resistance at the end of life.

Once the C_{eol} and $R_{s,eol}$ values have been established, the procedure can be applied according to the following steps:

1. The nominal characteristics of the battery pack cells are considered.
2. Starting from the relation $E_0 = E_0(DOD, T)$, where T is the temperature, the inverse relation $DOD = DOD(E_0, T)$ is obtained.
3. The battery pack is charged, the cell voltages in the modules are equalized, and the stabilization of the voltages and temperatures of the modules is awaited.
4. The BMS equalization function is disabled, and a standard discharge is performed.
5. After the voltages and temperatures of all cell groups are stabilized, the battery pack is recharged with CC/CV charging.

The modules' voltage curves for steps 4 and 5 are reported in Figure 6.

From the inverse relationship $DOD = DOD(E_0, T)$, it is, therefore, possible to identify the DOD values at the beginning and end of the discharge phase for each module, starting from the corresponding voltage values shown Figure 6. If Ah_{sc} is the cumulative charge delivered during discharge by the storage system (measured in ampere-hours), the effective capacity of the i -th module is given by

$$C_{eff_i} = \frac{Ah_{sc}}{DOD_{f_i} - DOD_{i_i}} \quad i = 1, \dots, n \quad (11)$$

where n is the number of modules in the storage system.

By applying (4) and (7), the values of the cycle energy efficiency η_E and the A_c area are calculated. The calculation of the ampere-hour efficiency (3) has been excluded from the discussion, because the currents absorbed by the electronics of the storage system could be comparable with those of the cells, which would invalidate the result. At the end of the test, for each module i , the following performance indices are available:

$$C_i, \eta_{E,i}, A_{c,i} \quad i = 1, \dots, n \quad (12)$$

The highest values of capacity and efficiency and the lowest values of $A_{c,i}$ correspond to the most-performant modules, i.e., with the lowest level of degradation. Using the nominal and end-of-life values for the resistance and the capacity in the equivalent circuit

shown in Figure 4, it is possible to derive the nominal reference values, $\eta_{E,nom}$ and $A_{c,nom}$, and end-of-life values, $\eta_{E,eol}$ and $A_{c,eol}$, for the parameters in (12).

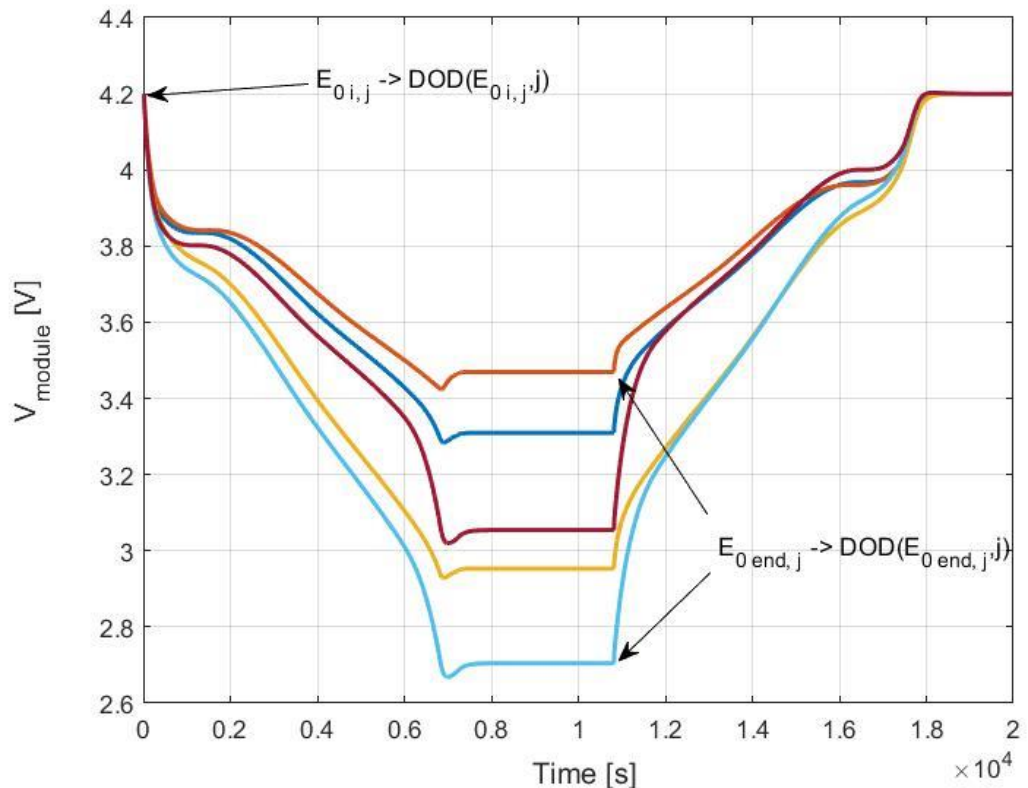


Figure 6. Discharge–charge voltage curve for pack modules.

The proposed degradation function has the following formulation and structure:

$$F_{deg_i} = P_1 \left(1 - \frac{C_i}{C_{nom}} \right) + P_2 \left(1 - \frac{\eta_E}{\eta_{E,nom}} \right) + P_3 \left(1 - \frac{A_{c,nom}}{A_{c,i}} \right) \quad (13)$$

The maximum value for the degradation function that leads to the withdrawal of the cells is defined as

$$F_{max} = P_1 \left(1 - \frac{C_{eol}}{C_{nom}} \right) + P_2 \left(1 - \frac{\eta_{E,eol}}{\eta_{E,nom}} \right) + P_3 \left(1 - \frac{A_{c,nom}}{A_{c,eol}} \right) \quad (14)$$

The weights of the individual contributions in (13) are determined based on the application, with P_1 related to the residual capacity (available energy), P_2 to the losses (series resistance and deliverable power), and P_3 to both capacity and resistance.

Based on the degradation function, the following situations can be identified:

$$F_{deg_i} = 0 \rightarrow \text{nominal condition of the module} \quad (15)$$

$$0 < F_{deg_i} < F_{max} \rightarrow \text{operative range for the module}$$

$$F_{deg_i} \geq F_{max} \rightarrow \text{EOL of the module}$$

The degradation function can be less than zero if the module has a better condition than the reference one. By carrying out the test during the operational life of the storage system, the degradation of the cells can be monitored, establishing whether a particular group presents an operating anomaly or whether the system is approaching the conditions of withdrawal from the application. Since $\eta_{E,nom}$, $A_{c,nom}$, $\eta_{E,eol}$, $A_{c,eol}$ depend on the charge-discharge current profiles, they should be determined at each test, using the equivalent

circuit of Figure 4, parameterized with the initial values of E_0 , C_{nom} , C_{eol} , $R_{s,nom}$, $R_{s,eol}$, which remain unchanged. Indeed, the charge–discharge current depends on the lower values for the capacity and the higher value for the resistance of the modules, which change with ageing. The parameters for the i -th modules at the n -th test $\eta_{E,i}^n$, $A_{c,i}^n$, C_i^n determine the current degradation function $F_{deg,i}^n$ in (13), to be compared with F_{max}^n , evaluated from (14) using the parameters C_{eol} , $\eta_{E,eol}^n$, $A_{c,eol}^n$.

We conducted a simulation to evaluate the degradation function for modules with different values of effective capacity and resistance due to the different performances of the cells in each of them. We used a degradation function, given in equation (16), for the test.

$$F_{deg} = 20 \left(1 - \frac{C}{C_{nom}} \right) + 10 \left(1 - \frac{\eta_E}{\eta_{E,nom}} \right) + 10 \left(1 - \frac{A_{c,nom}}{A_c} \right) \quad (16)$$

We calculated the degradation function for the basic performance, which has a value of zero, and for different values of the effective capacitance, impedance, and open-circuit voltage of each module. The results of the simulations are presented in Table 2. If the performance is better than the nominal reference, the value of the degradation function is negative. On the other hand, if the performance is worse than the nominal reference, the degradation function is greater than zero and increases as the deviation of the individual parameter from the nominal reference value becomes more severe.

Table 2. Simulation results for the degradation function with different deviations from the baseline performances.

| Module | Capacity | Open-Circuit Voltage | Impedance | Fdeg |
|-----------------------|----------|---------------------------------|-----------|-------|
| Baseline performances | Co | Eo(SOC) | Zo | 0 |
| Optimal | 1.12 Co | Eo(SOC) | 0.9 Zo | -4.18 |
| Reduced E0 | Co | Eo(SOC) $(1 - (0.12(1 - SOC)))$ | Zo | 2.441 |
| Reduced C | 0.94 Co | Eo(SOC) | Zo | 1.879 |
| Z max | Co | Eo(SOC) | 1.5 Zo | 5.072 |
| Reduced C + Z max | 0.94 Co | Eo(SOC) | 1.5 Zo | 7.253 |
| Reduced E0, C + Z max | 0.94 Co | Eo(SOC) $(1 - (0.12(1 - SOC)))$ | 1.5 Zo | 8.598 |

If it is not possible to carry out the standard discharge and recharge test, the procedure can still be applied to a discharge and recharge cycle that has the following characteristics:

6. At the beginning of the cycle, the voltages of all the modules must be at rest and identical to each other.
7. The temperatures of all modules must be in equilibrium and similar, within a predefined tolerance.
8. Before the start of the cycle, the BMS equalization system must be deactivated.
9. Discharging and charging must be in a quasi-stationary regime, with variation in the order of 0.1C/minute or less, except for the beginning and end of the discharging phase and the beginning of the charging phase.
10. The discharge and charge currents must not be too small, to contain the error on the F_{deg} parameters evaluation.
11. At the end of the discharge, the voltage should be measured when the cell voltages and temperatures have stabilized.
12. Charging must take place with the final part at a constant voltage (the BMS normally performs this setting by default, CC/CV charging).
13. At least one of the final voltages of the cell subgroups must be the same as the starting one.

3. Results

The following is a description of a real-world application designed to monitor the innovative charging station called the JuiceRoll Race Edition (JuiceRoll). This charging

infrastructure is specifically developed for the FIM Enel MotoE World Cup. It has been used since the first race of the third season of the competition, held in Jerez de la Frontera, Spain, on the 2 May 2021.

JuiceRoll is a racing charger composed of two interconnectable units called the semi-mobile unit (SMU) and the mobile unit (MU), each one with an integrated storage system. This device is highly innovative and decouples the input power needed from the grid from the output power given to the electric motorbikes during charging, significantly reducing the grid load.

The SMU is a semi-mobile unit with a 50 kW DC output, an AC input from the grid of up to 22 kW (but it also works with no grid input), and a 51 kWh embedded storage system. The MU is a moveable 10 kW DC charger also equipped with AC outputs (230 Vac at 50 Hz). Its 6 kWh embedded storage system allows the MU to charge the e-motorbikes on the starting grid and to supply power to their tire warmers while in transit to the pit lane and starting grid. Figure 7 illustrates the complete charger system (a), MU (b), and SMU (c).



Figure 7. JuiceRoll charger (a) complete system; (b) mobile unit; (c) semi-mobile unit.

The storage system is composed of modules connected in series, each one built of cells connected in parallel. Figure 8 shows the CAD model of the SMU and some of its parts.

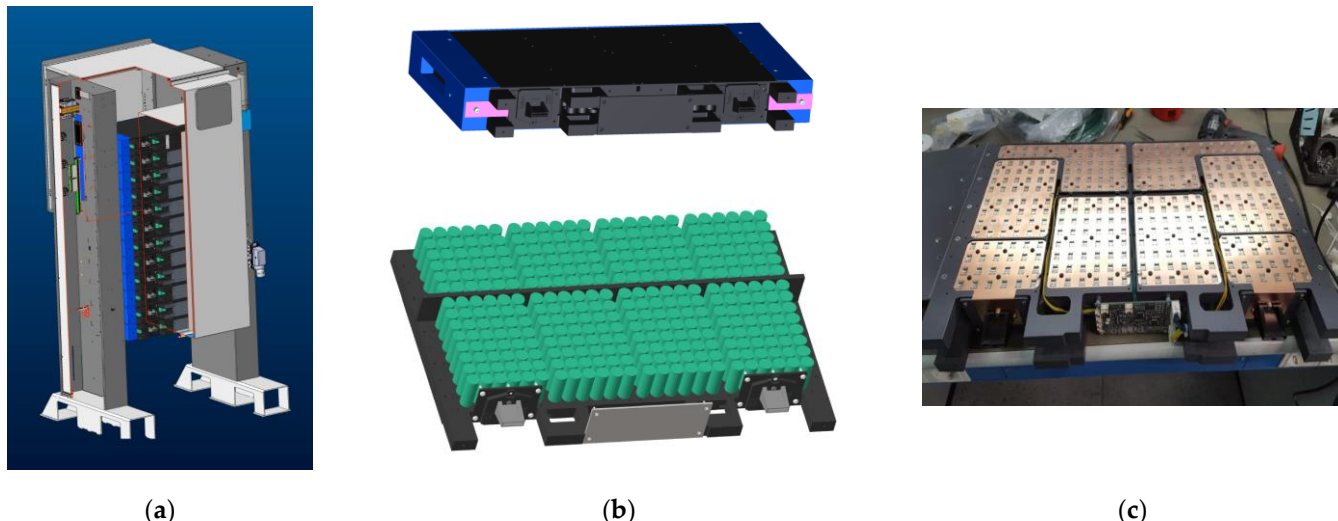


Figure 8. Storage system of the semi-mobile part. (a) Rack with modules; (b) detail of the module; (c) plates for parallel cell connections.

Table 3 shows the nominal electrical characteristics of the LG INR18650 MJ1 cells used to build the JuiceRoll storage system.

Table 3. Nominal characteristics of LG INR18650 MJ1 cells.

| Cell Model INR18650 MJ1-LG | Unit | Nominal Value |
|----------------------------|--------|---------------|
| Nominal Capacity | mAh | 3500 |
| Max Voltage | V | 4.20 |
| Nominal Voltage | V | 3.64 |
| Min Voltage | V | 2.70 |
| Max Charge Current | A | 3.4 |
| Suggested Charge Rate | C rate | 0.50 |
| Max Discharge Current | A | 10.0 |

The battery pack modules are assembled with submodules of cells in parallel, connected in series: Table 4 shows the characteristics and nominal values for the modules of the semi-mobile and mobile units.

Table 4. Nominal characteristics of the JuiceRoll modules.

| Characteristic | Unit | SMU Module 14S 24P | MU Module 56S 3P |
|-----------------------|------|--------------------|------------------|
| Nominal Capacity | Ah | 84.0 | 10.5 |
| Max Charge Current | A | 81.6 | 10.2 |
| Max Discharge Current | A | 240.0 | 30.0 |
| Max Voltage | V | 58.8 | 235.2 |
| Nominal Voltage | V | 50.9 | 203.6 |
| Min Voltage | V | 37.8 V | 151.2 |
| Module Nominal Energy | kWh | 4.27 | 2.14 |

The modules are assembled in series to create the final battery packs of both units, the characteristics of which are listed in Table 5.

Table 5. Nominal characteristics of SMU and MU battery packs.

| Characteristic | Unit | SMU Pack (12S Module) | MU Pack (3S Module) |
|------------------------------|------|-----------------------|---------------------|
| Max Charge Current | A | 81.6 | 10.2 |
| Suggested Max Charge Current | A | 40.8 | 5.1 |
| Max Discharge Current | A | 240.0 | 30.0 |
| Max Voltage | V | 705.6 | 705.6 |
| Nominal Voltage | V | 610.7 | 610.7 |
| Min Voltage | V | 453.6 | 453.6 |
| Nominal Energy | kWh | 51.30 | 6.41 |

The proposed procedure applies to the submodules of 24 and 3 cells in parallel that compose the modules of the SMU and MU, respectively.

The tests reported in the present document were carried out on one of the JuiceRoll prototypes, which presented operational problems: the storage system failed to provide its nominal energy in discharge since a submodule reached the minimum working voltage much earlier than others. The tests were carried out during the normal operation of the storage in uncontrolled temperature and humidity conditions. However, the location where the battery charger operated was a structure where temperature and humidity were almost constant, and the humidity was contained. Data acquisition during operation occurred at 1 s sampling intervals.

The procedure was customized to the case of the JuiceRoll; we carried out a test that consisted of a constant power discharge test followed by a pause and a CC/CV recharge. It should be underlined that in the case of the JuiceRoll, the final charging phase at constant voltage is carried out not by continuously decreasing the charging current, as usually happens, but through current pulses of 8 A and subsequent pauses. The test measurements were conducted under normal operating conditions, without conditioning the battery before the measurements. The test was indeed designed to be applied in uncontrolled working conditions.

At the end of the test, the following data were collected:

- Date;
- SOC;
- Lowest cell temperature [°C];
- Highest cell temperature [°C];
- Overall battery pack voltage [mV];
- Current read by LEM HSNDR200-S00 [mA];
- Highest cell voltage [mV];
- Cell lowest voltage [mV];
- Voltage difference between the highest and lowest cell [mV];
- Voltage [mV] and temperature [°C] of the 14 submodules that compose each of the 12 modules.

All data were sampled at a constant frequency, at a rate of 1 s. We waited approximately 60 min between the discharge and charging sessions, which allowed the battery pack to return to a temperature suitable for charging. The maximum temperature during charging is 45 °C; if this limit is hit, charging is inhibited until the temperature comes back below 43 °C. After the rest period, the cell voltage stabilized.

The current applied to the pack during the test is shown in Figure 9a; the positive current values correspond to recharging (absorbed current). The right tail of the curve in Figure 9a corresponds to the final charging phase, consisting of current pulses.

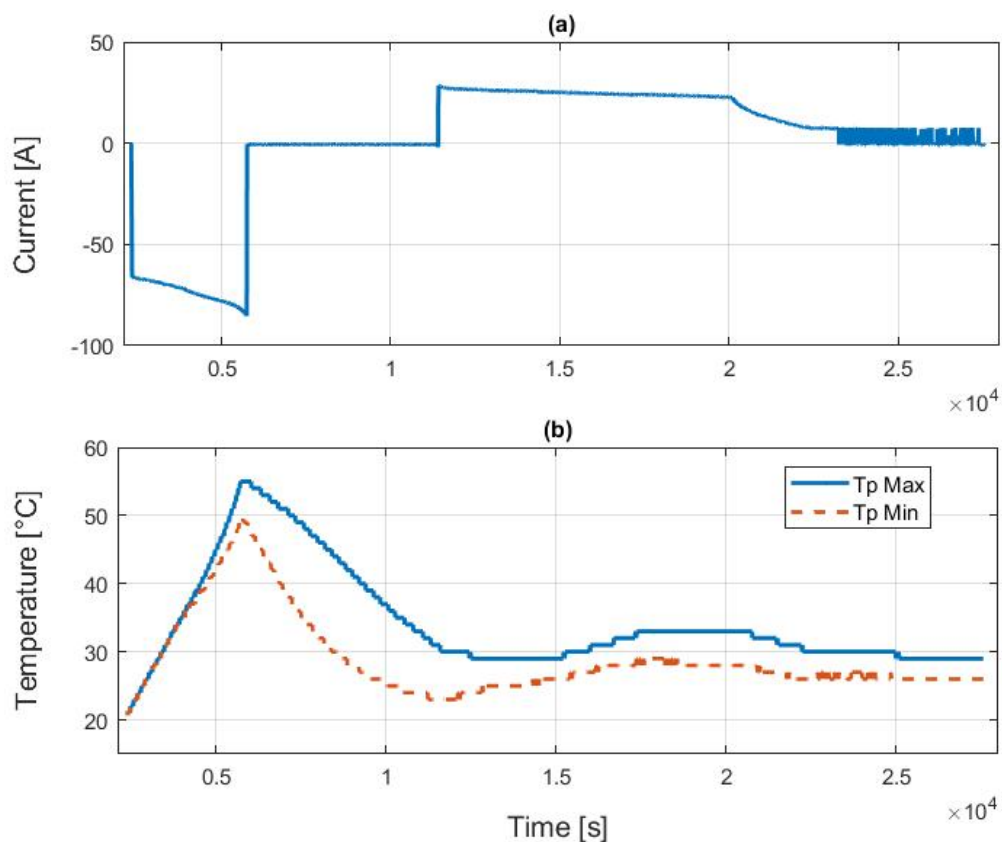


Figure 9. Discharge and recharge test: (a) current supplied/absorbed by the battery pack; (b) trend of maximum and minimum cell temperatures during the test.

A necessary condition to construct the degradation function is that the temperature of the cell groups at the pause points must be fairly homogeneous and not higher than a maximum of 40 $^{\circ}$ C. Figure 9b compares the trend of the maximum and minimum temperatures recorded throughout the test while the current depicted in Figure 9a flowed through the pack.

At the beginning of the test, the system is at rest; the cells' temperatures are equal to the ambient temperature. During the discharge, the system generates heat, and the temperatures of the cells increase unevenly. Subsequently, due to the combined effect of the pause phase and that of the fans, the temperatures dropped, reaching 23 $^{\circ}$ C for the minimum temperature and 30 $^{\circ}$ C for the maximum temperature, at the end of the pause phase. At the end of the test, the maximum temperature of the cells was 29 $^{\circ}$ C and the minimum was 26 $^{\circ}$ C.

Figure 10 reports the voltage values for the submodules corresponding to module 1, recorded during the test.

The procedure requires that the cells are at rest, i.e., that the current is zero and that the voltage and temperature do not vary over time, before the test begins, at the end of the pause phase, and at the end of the test. Figure 10 shows that these conditions were not fully realized in the present case. However, the resulting overall error is rather limited, as the numerical error in the evaluation of the open-circuit voltage in the first discharge phase is of the maximum order of 0.01 V, while in the pause phase, the maximum measurement error is approximately 0.02 V.

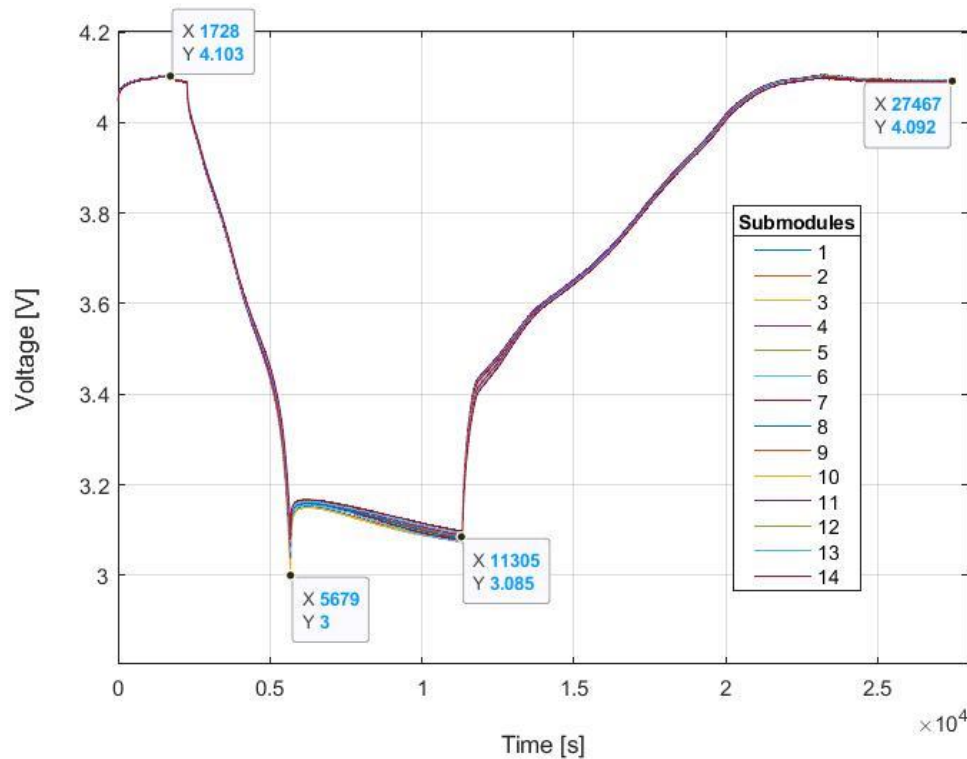


Figure 10. Discharge and recharge test—module 1 submodule voltages.

Data Processing and Experimental Test Results

The degradation function measures the performance loss of a generic cell or group of cells compared to a reference cell or group. In this specific case, two groups of reference cells were defined: one for module 1 and the other for the remaining JuiceRoll modules. Module 1, which houses the master unit of the BMS, operates differently from the others. Indeed, each module powers the associated BMS unit, while the master unit coordinates all the BMS units and communicates with the outside, absorbing much more current than the slave units. The two reference values for the degradation function were constructed by considering the average voltage trend of all the cells of module 1 and that of the remaining cells of the entire system.

Table 6 shows the estimate of the capacity of each submodule that composes the SMU battery. The capacities of the submodules whose degradation functions were the minimum (module 6, group 1) and maximum (module 12, group 10) at the end of the test are shown in bold red. The submodule with the greatest capacity is highlighted in bold (module 5, group 12).

Table 6. Estimated capacity of the submodule, Sub, for each module, Mod.

| Capacity [Ah] | Mod 1 | Mod 2 | Mod 3 | Mod 4 | Mod 5 | Mod 6 | Mod 7 | Mod 8 | Mod 9 | Mod 10 | Mod 11 | Mod 12 |
|---------------|-------|-------|-------|-------|--------------|-------|-------|-------|-------|--------|--------|--------|
| Sub 1 | 80.00 | 81.16 | 81.28 | 81.70 | 81.34 | 81.62 | 81.24 | 81.54 | 81.37 | 81.76 | 81.50 | 81.59 |
| Sub 2 | 80.01 | 81.60 | 81.19 | 80.99 | 81.16 | 81.59 | 81.25 | 81.57 | 81.37 | 81.70 | 81.04 | 81.58 |
| Sub 3 | 80.22 | 81.51 | 81.37 | 81.52 | 80.81 | 81.16 | 81.36 | 81.48 | 81.32 | 81.16 | 81.32 | 81.61 |
| Sub 4 | 80.40 | 81.49 | 81.35 | 81.29 | 81.24 | 81.24 | 81.23 | 81.05 | 81.46 | 81.62 | 81.32 | 81.03 |
| Sub 5 | 80.40 | 81.52 | 81.30 | 81.21 | 81.20 | 81.13 | 81.18 | 81.31 | 80.98 | 80.86 | 81.34 | 81.45 |
| Sub 6 | 80.22 | 80.79 | 81.10 | 81.44 | 81.24 | 81.46 | 81.08 | 81.21 | 81.44 | 81.60 | 80.83 | 81.48 |
| Sub 7 | 80.31 | 81.52 | 81.42 | 80.88 | 80.82 | 81.28 | 81.13 | 81.17 | 81.39 | 81.57 | 80.84 | 81.62 |
| Sub 8 | 80.74 | 80.83 | 81.50 | 81.38 | 81.07 | 81.09 | 81.11 | 81.14 | 81.48 | 81.60 | 81.65 | 80.94 |
| Sub 9 | 80.78 | 81.26 | 80.82 | 80.81 | 80.86 | 80.88 | 81.14 | 81.14 | 81.16 | 81.29 | 81.00 | 81.34 |
| Sub 10 | 80.82 | 81.30 | 81.35 | 80.83 | 80.76 | 81.04 | 81.57 | 81.18 | 81.59 | 81.01 | 80.90 | 79.12 |
| Sub 11 | 80.48 | 81.14 | 81.36 | 80.75 | 81.13 | 80.96 | 81.33 | 81.04 | 81.57 | 81.26 | 81.46 | 81.36 |
| Sub 12 | 80.71 | 81.32 | 81.60 | 80.78 | 81.77 | 80.96 | 81.73 | 81.04 | 81.65 | 81.00 | 81.11 | 80.91 |
| Sub 13 | 80.65 | 81.19 | 81.59 | 81.21 | 81.67 | 81.29 | 81.67 | 80.82 | 81.60 | 81.64 | 81.83 | 80.99 |
| Sub 14 | 81.05 | 81.01 | 81.00 | 80.87 | 81.30 | 81.01 | 81.38 | 81.08 | 81.25 | 81.00 | 81.73 | 80.89 |

Table 7 shows the efficiency of the discharge and recharge cycle for each submodule.

Table 7. Efficiency of the discharge–charge cycle.

| Efficiency | Mod 1 | Mod 2 | Mod 3 | Mod 4 | Mod 5 | Mod 6 | Mod 7 | Mod 8 | Mod 9 | Mod 10 | Mod 11 | Mod 12 |
|------------|-------|-------|-------|-------|-------|-------|-------|-------|-------|--------|--------|--------|
| Sub 1 | 0.97 | 0.98 | 0.97 | 0.98 | 0.97 | 0.98 | 0.97 | 0.98 | 0.97 | 0.98 | 0.97 | 0.98 |
| Sub 2 | 0.97 | 0.98 | 0.97 | 0.97 | 0.98 | 0.97 | 0.97 | 0.97 | 0.97 | 0.98 | 0.97 | 0.98 |
| Sub 3 | 0.97 | 0.98 | 0.97 | 0.98 | 0.97 | 0.98 | 0.97 | 0.97 | 0.97 | 0.97 | 0.97 | 0.98 |
| Sub 4 | 0.97 | 0.97 | 0.97 | 0.97 | 0.97 | 0.97 | 0.97 | 0.97 | 0.97 | 0.97 | 0.97 | 0.97 |
| Sub 5 | 0.97 | 0.98 | 0.97 | 0.98 | 0.97 | 0.98 | 0.97 | 0.97 | 0.97 | 0.97 | 0.97 | 0.98 |
| Sub 6 | 0.97 | 0.98 | 0.97 | 0.98 | 0.97 | 0.98 | 0.97 | 0.97 | 0.97 | 0.98 | 0.97 | 0.98 |
| Sub 7 | 0.97 | 0.98 | 0.97 | 0.98 | 0.97 | 0.98 | 0.97 | 0.98 | 0.97 | 0.98 | 0.97 | 0.98 |
| Sub 8 | 0.97 | 0.97 | 0.98 | 0.97 | 0.98 | 0.98 | 0.97 | 0.98 | 0.97 | 0.98 | 0.97 | 0.98 |
| Sub 9 | 0.97 | 0.97 | 0.97 | 0.97 | 0.98 | 0.97 | 0.97 | 0.97 | 0.97 | 0.97 | 0.97 | 0.98 |
| Sub 10 | 0.97 | 0.97 | 0.98 | 0.97 | 0.98 | 0.98 | 0.97 | 0.97 | 0.97 | 0.97 | 0.97 | 0.97 |
| Sub 11 | 0.97 | 0.97 | 0.97 | 0.97 | 0.97 | 0.97 | 0.97 | 0.97 | 0.97 | 0.97 | 0.97 | 0.97 |
| Sub 12 | 0.97 | 0.97 | 0.98 | 0.97 | 0.98 | 0.97 | 0.98 | 0.97 | 0.98 | 0.97 | 0.98 | 0.97 |
| Sub 13 | 0.97 | 0.97 | 0.98 | 0.97 | 0.98 | 0.97 | 0.98 | 0.97 | 0.98 | 0.97 | 0.98 | 0.97 |
| Sub 14 | 0.98 | 0.97 | 0.98 | 0.97 | 0.98 | 0.97 | 0.98 | 0.97 | 0.98 | 0.97 | 0.98 | 0.97 |

Table 8 reports the values for the areas of the hysteresis curves for the submodules.

Table 8. Hysteresis curve areas.

| A _c | Mod 1 | Mod 2 | Mod 3 | Mod 4 | Mod 5 | Mod 6 | Mod 7 | Mod 8 | Mod 9 | Mod 10 | Mod 11 | Mod 12 |
|----------------|-------|-------|-------|-------|-------|-------|-------|-------|-------|--------|--------|--------|
| Sub 1 | 0.105 | 0.076 | 0.091 | 0.073 | 0.096 | 0.069 | 0.094 | 0.077 | 0.096 | 0.076 | 0.093 | 0.071 |
| Sub 2 | 0.110 | 0.078 | 0.098 | 0.082 | 0.100 | 0.074 | 0.101 | 0.082 | 0.101 | 0.080 | 0.100 | 0.075 |
| Sub 3 | 0.108 | 0.075 | 0.093 | 0.076 | 0.098 | 0.074 | 0.096 | 0.082 | 0.099 | 0.083 | 0.095 | 0.073 |
| Sub 4 | 0.109 | 0.087 | 0.097 | 0.088 | 0.099 | 0.084 | 0.104 | 0.094 | 0.103 | 0.093 | 0.101 | 0.086 |
| Sub 5 | 0.095 | 0.078 | 0.082 | 0.079 | 0.085 | 0.076 | 0.087 | 0.085 | 0.089 | 0.085 | 0.085 | 0.075 |
| Sub 6 | 0.096 | 0.082 | 0.086 | 0.081 | 0.087 | 0.075 | 0.089 | 0.084 | 0.088 | 0.081 | 0.089 | 0.075 |
| Sub 7 | 0.093 | 0.078 | 0.083 | 0.082 | 0.086 | 0.074 | 0.084 | 0.082 | 0.084 | 0.081 | 0.087 | 0.075 |
| Sub 8 | 0.088 | 0.084 | 0.080 | 0.083 | 0.081 | 0.079 | 0.081 | 0.086 | 0.082 | 0.084 | 0.078 | 0.080 |
| Sub 9 | 0.089 | 0.086 | 0.082 | 0.088 | 0.085 | 0.082 | 0.084 | 0.087 | 0.085 | 0.086 | 0.084 | 0.080 |
| Sub 10 | 0.088 | 0.084 | 0.078 | 0.084 | 0.082 | 0.080 | 0.082 | 0.086 | 0.084 | 0.089 | 0.083 | 0.102 |
| Sub 11 | 0.097 | 0.099 | 0.087 | 0.101 | 0.091 | 0.095 | 0.092 | 0.104 | 0.090 | 0.104 | 0.090 | 0.095 |
| Sub 12 | 0.085 | 0.094 | 0.075 | 0.096 | 0.078 | 0.090 | 0.080 | 0.098 | 0.079 | 0.099 | 0.080 | 0.092 |
| Sub 13 | 0.088 | 0.099 | 0.079 | 0.098 | 0.081 | 0.092 | 0.081 | 0.103 | 0.081 | 0.099 | 0.081 | 0.093 |
| Sub 14 | 0.081 | 0.094 | 0.075 | 0.095 | 0.075 | 0.088 | 0.076 | 0.094 | 0.077 | 0.095 | 0.075 | 0.088 |

The results show how the efficiency is very high and similar for all submodules. In fact, in the test condition, the efficiency values were not very sensitive to variations of up to approximately 30% of the cell resistance, as demonstrated by the simulations.

The degradation function is obtained by adding a series of parameters, appropriately weighted according to the specific application, estimated from the discharge and recharge test. In the present case, the application was not power-demanding but required the modules to deliver the maximum possible energy. For this reason, the weight of the capacity term determined 50% of the degradation function, as reported in Equation (16). Moreover, in the present case, the nominal values were replaced by the average values of the analyzed parameters. Table 9 shows the numerical value of the degradation function estimated for each submodule.

Table 9. Degradation function value for each submodule.

| Fdeg | Mod 1 | Mod 2 | Mod 3 | Mod 4 | Mod 5 | Mod 6 | Mod 7 | Mod 8 | Mod 9 | Mod 10 | Mod 11 | Mod 12 |
|--------|-------|-------|-------|-------|-------|-------|-------|-------|-------|--------|--------|--------|
| Sub 1 | 1.05 | -1.27 | 0.50 | -1.71 | 1.07 | -2.19 | 0.84 | -1.21 | 1.06 | -1.32 | 0.73 | -1.95 |
| Sub 2 | 1.64 | -1.04 | 1.45 | -0.41 | 1.68 | -1.61 | 1.79 | -0.61 | 1.76 | -0.84 | 1.67 | -1.40 |
| Sub 3 | 1.28 | -1.37 | 0.70 | -1.33 | 1.53 | -1.50 | 1.16 | -0.58 | 1.48 | -0.37 | 1.00 | -1.67 |
| Sub 4 | 1.40 | 0.06 | 1.25 | 0.17 | 1.51 | -0.23 | 2.07 | 1.01 | 1.94 | 0.71 | 1.77 | 0.05 |
| Sub 5 | -0.28 | -1.09 | -0.50 | -0.88 | -0.18 | -1.21 | 0.09 | -0.20 | 0.40 | -0.04 | -0.17 | -1.44 |
| Sub 6 | 0.03 | -0.41 | -0.05 | -0.72 | 0.12 | -1.39 | 0.32 | -0.21 | 0.14 | -0.72 | 0.45 | -1.36 |
| Sub 7 | -0.30 | -1.02 | -0.48 | -0.43 | 0.01 | -1.48 | -0.20 | -0.50 | -0.35 | -0.70 | 0.21 | -1.41 |
| Sub 8 | -0.99 | -0.17 | -0.85 | -0.43 | -0.59 | -0.80 | -0.61 | -0.07 | -0.65 | -0.33 | -1.09 | -0.70 |
| Sub 9 | -0.84 | -0.11 | -0.37 | 0.31 | -0.09 | -0.48 | -0.30 | 0.15 | -0.11 | -0.01 | -0.25 | -0.79 |
| Sub 10 | -0.99 | -0.37 | -1.07 | -0.21 | -0.41 | -0.66 | -0.56 | -0.05 | -0.43 | 0.39 | -0.34 | 2.40 |
| Sub 11 | 0.07 | 1.55 | 0.04 | 1.88 | 0.54 | 1.12 | 0.70 | 2.13 | 0.29 | 2.06 | 0.35 | 1.00 |
| Sub 12 | -1.29 | 0.93 | -1.49 | 1.27 | -1.14 | 0.52 | -0.93 | 1.43 | -1.00 | 1.56 | -0.70 | 0.69 |
| Sub 13 | -0.95 | 1.54 | -0.92 | 1.41 | -0.70 | 0.69 | -0.75 | 2.07 | -0.72 | 1.42 | -0.76 | 0.89 |
| Sub 14 | -1.78 | 0.90 | -1.33 | 1.14 | -1.33 | 0.23 | -1.25 | 0.93 | -1.07 | 1.06 | -1.47 | 0.29 |

As mentioned, the first column of the table expresses an F_{deg} value relating to the submodules of module 1, while the other columns relate to the remaining 154 submodules. A direct comparison between the values of the first column and the subsequent ones is, therefore, not possible.

A negative value of F_{deg} implies that the submodule has better characteristics/performances (effective cell capacity, cycle efficiency, etc.) than those of the reference group (average values over the modules); $F_{deg} = 0$ implies that they coincide, and $F_{deg} > 0$ that they are worse. Submodule 10 of module 12 is the one with the worst performance.

The graph in Figure 11 illustrates the voltage trends of each submodule in module 12. Analyzing the curves helps us understand the behavior of the group being studied, revealing a heavily damaged submodule.

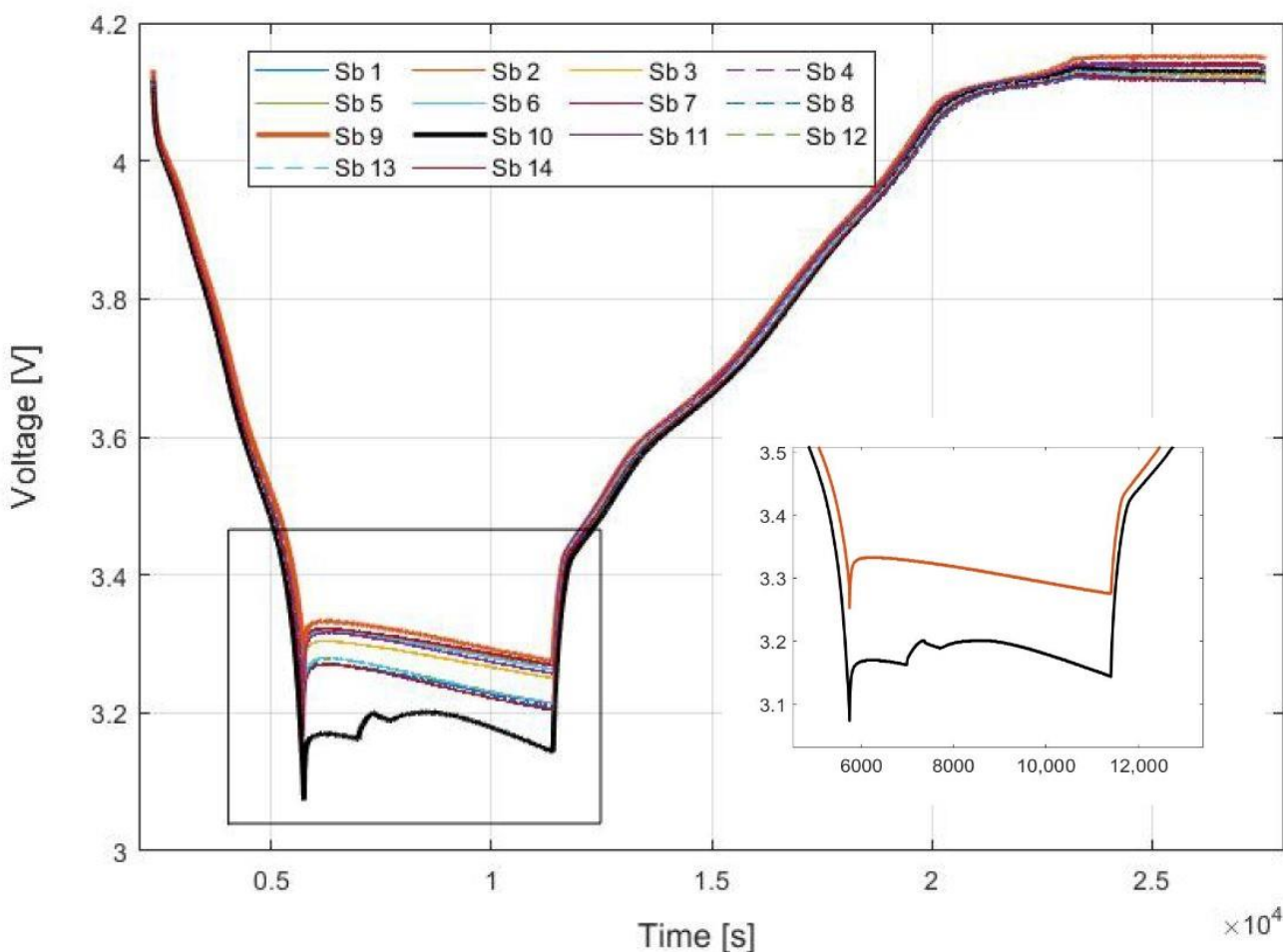


Figure 11. Discharge voltage curves for the module 12 groups of cells. Inset: detail of the pause phase for the most (submodule 9) and least (submodule 10) performant submodules.

Figure 11 indicates that submodule 10 of module 12 has a lower capacity than the others, as its discharge voltage was consistently lower. Additionally, it entered the non-linear zone much earlier than the ‘average group’. During the pause phase, there was an anomalous behavior in the voltage curve for submodule 10, which could be explained by an anomaly in one of the cells. This cell may have been discharging on the others, possibly due to issues related to the cooling of a contact resistance.

Similarly, the hysteresis curve for submodule 10 shows a notable deviation from the one for submodule 9, as shown in Figure 12. For comparison, the graph also reports the average value for the entire module 12, with the exclusion of the most damaged submodule.

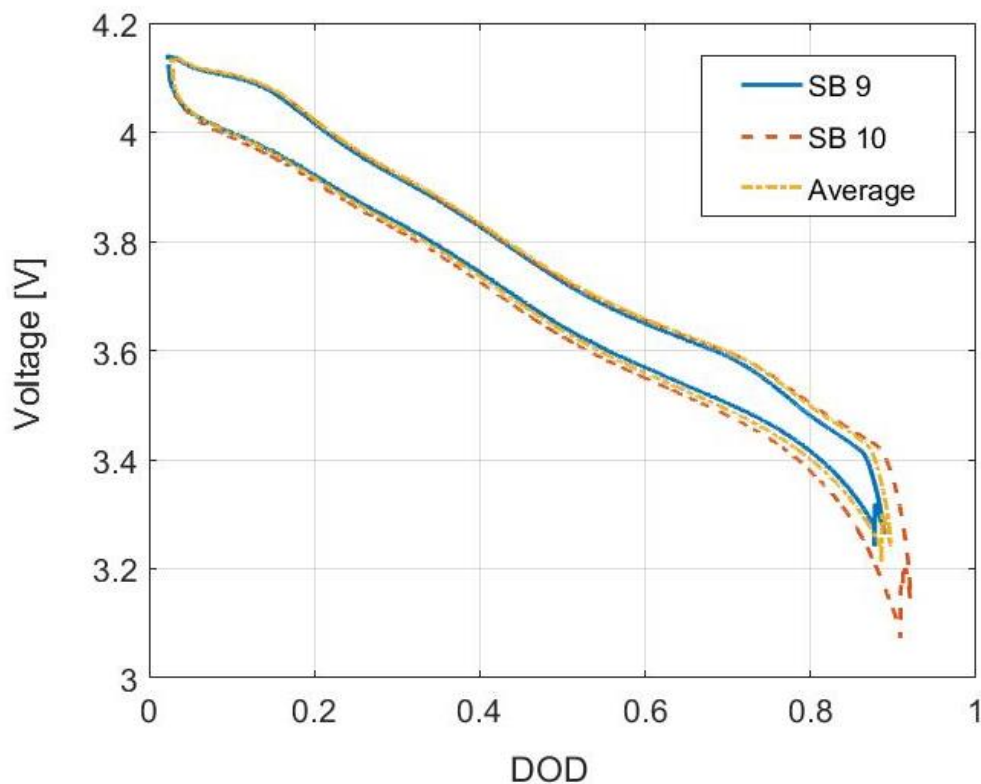


Figure 12. Hysteresis curves for submodule 9 (solid blue line) and 10 (dashed red line) of module 12. The average value of the hysteresis curve is shown for comparison (dotted yellow line).

The degradation of the module, as indicated by the degradation index, was subsequently verified by directly inspecting the isolated module that had been removed from the system. The degradation was found to be the result of a vibration test that had caused physical damage to one of the cells as part of a prior study on the system.

4. Discussion

This paper presents a test procedure for evaluating the performances of modules composing a battery pack using the charger's converter and the battery BMS, without the need for complex instrumentation. This method has the advantage of not requiring additional instrumentation beyond what is needed for a standard capacity test of a battery pack.

In a system consisting of a series of modules, each comprising cells placed in parallel, the method allows characterization of the state of degradation of each module compared to reference performances. It can identify any components that need replacement or determine when the entire system should be retired after its first or second use.

The method has been validated through numerical simulations and experimental tests and has been successfully employed for diagnostic purposes in the industrial field on damaged systems. The procedure was tested in a real-world case study, monitoring a battery storage system integrated in a charger called the JuiceRoll Race Edition. The goal was to identify any modules that may have aged prematurely or exhibited reliability issues.

The principal characteristics of the procedure are that it is non-destructive and does not require any disassembly of the battery pack. Moreover, the procedure can identify a variety of battery health issues, including capacity fade, impedance increase, and cell imbalance. It can track the health of the battery pack over time and identify any groups that may need to be replaced.

The procedure can be used for a variety of battery pack applications, including electric vehicles, renewable energy storage, and uninterruptible power supplies (UPSs).

The quantification of the accuracy and reliability of this method is ongoing. The method was, in fact, applied to multiple JuiceRoll BESS units, and managed to detect any anomalies present over time. However, the raw data are still being processed.

The limitations of the proposed procedure are the use of quasi-stationary charges and discharges, and closed cycles. Furthermore, the methodology requires that the slope of the open voltage curve as a function of the state of charge be such that an inverse relationship exists. Thus, the procedure is not applicable if the curve is particularly flat, as for lithium–iron–phosphate cells. Future developments concern the extension of the procedure to allow the calculation of degradation functions starting from the normal operating cycles of battery packs.

5. Patents

European Patent Application No. 22 189 126.0-1202, Ref. P3799EP00 11.01.2024.

Author Contributions: Conceptualization, M.P. and A.V.; methodology, M.P., F.V. and N.A.; software, M.P.; validation, M.P. and A.V.; formal analysis, M.P., F.V. and N.A.; investigation, M.P. and A.V.; resources, M.P. and A.V.; data curation, M.P. and A.V.; writing—original draft preparation, M.P.; writing—review and editing, N.A.; visualization, N.A.; supervision, F.V.; project administration, M.P. All authors have read and agreed to the published version of the manuscript.

Funding: This research received no external funding.

Data Availability Statement: The data presented in this study are available on request from the corresponding author. The data are not publicly available due to NDA commitments.

Conflicts of Interest: Author Alberto Venanzoni was employed by the company Enel X. The remaining authors declare that the research was conducted in the absence of any commercial or financial relationships that could be construed as a potential conflict of interest.

References

1. Nuoldayeva, G.; Serik, Y.; Adair, D.; Uzakbaiuly, B.; Bakenov, Z. State of Health Estimation Methods for Lithium-Ion Batteries. *Int. J. Energy Res.* **2023**, *2023*, 4297545. [[CrossRef](#)]
2. Chen, L.; Lü, Z.; Lin, W.; Li, J.; Pan, H. A new state-of-health estimation method for lithium-ion batteries through the intrinsic relationship between ohmic internal resistance and capacity. *Measurement* **2018**, *116*, 586–595. [[CrossRef](#)]
3. Che, Y.; Hu, X.; Lin, X.; Guo, J.; Teodorescu, R. Health prognostics for lithium-ion batteries: Mechanisms, methods, and prospects. *Energy Environ. Sci.* **2023**, *16*, 338–371. [[CrossRef](#)]
4. Huang, S.-C.; Tseng, K.-H.; Liang, J.-W.; Chang, C.-L.; Pecht, M. An Online SOC and SOH Estimation Model for Lithium-Ion Batteries. *Energies* **2017**, *10*, 512. [[CrossRef](#)]
5. Li, C.; Zhang, H.; Ding, P.; Yang, S.; Bai, Y. Deep feature extraction in lifetime prognostics of lithium-ion batteries: Advances, challenges and perspectives. *Renew. Sustain. Energy Rev.* **2023**, *184*, 113576. [[CrossRef](#)]
6. Locorotondo, E.; Cultrera, V.; Pugi, L.; Berzi, L.; Pasquali, M.; Andrenacci, N.; Lutzemberger, G.; Pierini, M. Electrical lithium battery performance model for second life applications. In Proceedings of the 2020 IEEE International Conference on Environment and Electrical Engineering and 2020 IEEE Industrial and Commercial Power Systems Europe (EEEIC/I&CPS Europe), Madrid, Spain, 9–12 June 2020; pp. 1–6. [[CrossRef](#)]
7. Semeraro, C.; Caggiano, M.; Olabi, A.-G.; Dassisti, M. Battery monitoring and prognostics optimization techniques: Challenges and opportunities. *Energy* **2022**, *255*, 124538. [[CrossRef](#)]
8. Li, J.; Adewuyi, K.; Lotfi, N.; Landers, R.G.; Park, J. A single particle model with chemical/mechanical degradation physics for lithium ion battery State of Health (SOH) estimation. *Appl. Energy* **2018**, *212*, 1178–1190. [[CrossRef](#)]
9. Wu, L.; Lyu, Z.; Huang, Z.; Zhang, C.; Wei, C. Physics-based battery SOC estimation methods: Recent advances and future perspectives. *J. Energy Chem.* **2024**, *89*, 27–40. [[CrossRef](#)]
10. Sihvo, J.; Roinila, T.; Stroe, D.-I. SOH analysis of Li-ion battery based on ECM parameters and broadband impedance measurements. In Proceedings of the IECON 2020 the 46th Annual Conference of the IEEE Industrial Electronics Society, Singapore, 18–21 October 2020; pp. 1923–1928. [[CrossRef](#)]
11. Feng, T.; Yang, L.; Zhao, X.; Zhang, H.; Qiang, J. Online identification of lithium-ion battery parameters based on an improved equivalent-circuit model and its implementation on battery state-of-power prediction. *J. Power Sources* **2015**, *281*, 192–203. [[CrossRef](#)]
12. Meng, J.; Luo, G.; Ricco, M.; Swierczynski, M.; Stroe, D.-I.; Teodorescu, R. Overview of Lithium-Ion Battery Modeling Methods for State-of-Charge Estimation in Electrical Vehicles. *Appl. Sci.* **2018**, *8*, 659. [[CrossRef](#)]

13. Zhu, C.; He, Z.; Bao, Z.; Sun, C.; Gao, M. Prognosis of Lithium-Ion Batteries' Remaining Useful Life Based on a Sequence-to-Sequence Model with Variational Mode Decomposition. *Energies* **2023**, *16*, 803. [[CrossRef](#)]
14. Zhao, J.; Feng, X.; Pang, Q.; Wang, J.; Lian, Y.; Ouyang, M.; Burke, A.F. Battery prognostics and health management from a machine learning perspective. *J. Power Sources* **2023**, *581*, 233474. [[CrossRef](#)]
15. Haskara, I.; Hegde, B.; Chang, C.-F. Reinforcement learning based EV energy management for integrated traction and cabin thermal management considering battery aging. *IFAC-PapersOnLine* **2022**, *55*, 348–353. [[CrossRef](#)]
16. de Beaulieu, M.H.; Jha, M.S.; Garnier, H.; Cerbah, F. Unsupervised Remaining Useful Life Prediction through Long Range Health Index Estimation based on Encoders-Decoders. *IFAC-PapersOnLine* **2022**, *55*, 718–723. [[CrossRef](#)]
17. Wang, Z.; Yang, F.; Xu, Q.; Wang, Y.; Yan, H.; Xie, M. Capacity estimation of lithium-ion batteries based on data aggregation and feature fusion via graph neural network. *Appl. Energy* **2023**, *336*, 120808. [[CrossRef](#)]
18. Yu, H.; Zhang, Z.; Yang, K.; Zhang, L.; Wang, W.; Yang, S.; Li, J.; Liu, X. Physics-informed ensemble deep learning framework for improving state of charge estimation of lithium-ion batteries. *J. Energy Storage* **2023**, *73*, 108915. [[CrossRef](#)]
19. Cui, B.; Wang, H.; Li, R.; Xiang, L.; Zhao, H.; Xiao, R.; Li, S.; Liu, Z.; Yin, G.; Cheng, X.; et al. Ultra-early prediction of lithium-ion battery performance using mechanism and data-driven fusion model. *Appl. Energy* **2024**, *353*, 122080. [[CrossRef](#)]
20. Zhang, H.; Hong, J.; Wang, Z.; Wu, G. State-Partial Accurate Voltage Fault Prognosis for Lithium-Ion Batteries Based on Self-Attention Networks. *Energies* **2022**, *15*, 8458. [[CrossRef](#)]
21. Dubarry, M.; Beck, D. Analysis of Synthetic Voltage vs. Capacity Datasets for Big Data Li-ion Diagnosis and Prognosis. *Energies* **2021**, *14*, 2371. [[CrossRef](#)]
22. Li, X.; Wang, Z.; Yan, J. Prognostic health condition for lithium battery using the partial incremental capacity and Gaussian process regression. *J. Power Sources* **2019**, *421*, 56–67. [[CrossRef](#)]
23. Zhang, S.; Zhai, B.; Guo, X.; Wang, K.; Peng, N.; Zhang, X. Synchronous estimation of state of health and remaining useful lifetime for lithium-ion battery using the incremental capacity and artificial neural networks. *J. Energy Storage* **2019**, *26*, 100951. [[CrossRef](#)]
24. Ma, G.; Zhang, Y.; Cheng, C.; Zhou, B.; Hu, P.; Yuan, Y. Remaining useful life prediction of lithium-ion batteries based on false nearest neighbors and a hybrid neural network. *Appl. Energy* **2019**, *253*, 113626. [[CrossRef](#)]
25. Bai, G.; Su, Y.; Rahman, M.M.; Wang, Z. Prognostics of Lithium-Ion batteries using knowledge-constrained machine learning and Kalman filtering. *Reliab. Eng. Syst. Saf.* **2023**, *231*, 108944. [[CrossRef](#)]
26. Diao, W.; Jiang, J.; Zhang, C.; Liang, H.; Pecht, M. Energy state of health estimation for battery packs based on the degradation and inconsistency. *Energy Procedia* **2017**, *142*, 3578–3583. [[CrossRef](#)]
27. Fan, J.; Zou, Y.; Zhang, X.; Guo, H. A novel State of Health estimation method for Lithium-ion battery in electric vehicles. *J. Phys. Conf. Ser.* **2019**, *1187*, 022014. [[CrossRef](#)]
28. Klintberg, A.; Klintberg, E.; Fridholm, B.; Kuusisto, H.; Wik, T. Statistical modeling of OCV-curves for aged battery cells. *IFAC-PapersOnLine* **2017**, *50*, 2164–2168. [[CrossRef](#)]
29. Vichard, L.; Ravey, A.; Venet, P.; Harel, F.; Pelissier, S.; Hissel, D. A method to estimate battery SOH indicators based on vehicle operating data only. *Energy* **2021**, *225*, 120235. [[CrossRef](#)]
30. Zhou, D.; Fu, P.; Yin, H.; Xie, W.; Feng, S. A Study of Online State-of-Health Estimation Method for In-Use Electric Vehicles Based on Charge Data. *IEICE Trans. Inf. Syst.* **2019**, *E102*, 1302–1309. [[CrossRef](#)]
31. Hong, J.; Wang, Z.; Chen, W.; Wang, L.; Lin, P.; Qu, C. Online accurate state of health estimation for battery systems on real-world electric vehicles with variable driving conditions considered. *J. Clean. Prod.* **2021**, *294*, 125814. [[CrossRef](#)]
32. Cacciato, M.; Nobile, G.; Scarella, G.; Scelba, G. Real-Time Model-Based Estimation of SOC and SOH for Energy Storage Systems. *IEEE Trans. Power Electron.* **2017**, *32*, 794–803. [[CrossRef](#)]

Disclaimer/Publisher's Note: The statements, opinions and data contained in all publications are solely those of the individual author(s) and contributor(s) and not of MDPI and/or the editor(s). MDPI and/or the editor(s) disclaim responsibility for any injury to people or property resulting from any ideas, methods, instructions or products referred to in the content.